npj | digital medicine

Article

Published in partnership with Seoul National University Bundang Hospital

https://doi.org/10.1038/s41746-026-02488-7

Imaging-based organ-specific aging clock predicts human diseases and mortality

Peng Ren[1,2,8], Wenjing Su[1,2,8], Jia You[1,2,8], Ying Liang[1,2], Weikang Gong[3,4], Wei Zhang[1,2], Zairen Zhou[1,2], Fei Dai[1], Xiaohe Hou[1,2], Wei-Shi Liu[1,2], Jianfeng Feng[1,2,5], He Wang[1,6] ✉, Jin-Tai Yu[1] ✉ & Wei Cheng[1,2,7] ✉

Organ-specific aging clocks hold great potential in reflecting organ health. In vivo imaging is inherently organ-specific and delineates structural and functional characteristics more objectively. However, there is no systematic evaluation of imaging-based aging clocks. We utilized 1777 imaging-derived phenotypes (IDPs) from 11,000 healthy participants and assessed the organ-specific biological age of seven organs. The organ-specific age gap was primarily associated with incident diseases and mortality related to corresponding organs. The top-contributing IDPs to organ-specific biological age emerged as biomarkers for incident disease predictions, achieving an area under the curve (AUC) greater than 0.8 for dementia (AUC = 0.82). Subsequent proteomic analysis revealed 966 shared and 507 organ-specific molecular signatures for the aging of different organs. Finally, we identified key modifiable factors and 14 drug targets for organ-specific aging. The imaging-based aging clocks demonstrate organ-specificity at both macro and micro scales, which could promote personalized intervention and treatment of organ aging.

Human aging, commonly characterized as biological age, is a heterogeneous process that differs not only between individuals but also between different organs[1]. By comparing the biological age to chronological age, i.e., age gap, insights could be given to whether specific organs exhibit accelerated or delayed aging relative to normal peers[2,3]. Elucidating such organ aging patterns could inform future risk of organ-specific diseases and facilitate potential early intervention to delay the aging process[2].

While a significant number of studies focused on measuring whole-body aging, few of them accounted for the heterogeneity across different organs. Recent organ-specific biological ages have been developed based on either empirical knowledge of pre-defined organ markers[4] or organ-enriched molecules using in vitro tissues[5,6]. Such frameworks could be refined by leveraging more objective organ markers. Specifically, in vivo imaging-based measurements are inherently organ-specific and could delineate structural and functional characteristics more objectively. In particular, magnetic resonance imaging (MRI)-based measurements have been increasingly utilized to capture brain aging[7–9], which exhibit clinical promise in identifying individuals at high risk of neurodegenerative diseases and monitoring the progression of diseases[8,10]. However, there is a lack of imaging-based aging clocks across other organs. We anticipate that age modelling with imaging-derived phenotypes could enhance organ specificity and reinforce their clinical relevance.

In such a situation, many important questions remain to be solved to comprehensively interrogate the applicability of organ-specific aging clocks in a large-scale, longitudinal cohort. What is the relationship between the aging clocks of different organs? Do organ-specific aging clocks contribute more to diseases and mortality of the corresponding organs? Will the imaging-based organ aging clocks also exhibit associations with peripheral organ-specific molecules? What are the potential modifiable factors and drug targets for the aging clocks of different organs?

To address the questions mentioned above, this study utilized 1777 IDPs obtained through MRI, optical coherence tomography (OCT), and dual-energy x-ray absorptiometry (DXA) from 11,000 healthy individuals in the UK Biobank (UKB). Seven organ-specific aging clocks for brain, heart, liver, kidney, pancreas, eye, and body composition were established through machine learning. This study aimed to (1) quantify the interrelationships between age gaps across multiple organs; (2) evaluate whether organ age gap is associated with and predictive of 48 incident diseases and five mortality;

[1]Institute of Science and Technology for Brain-Inspired Intelligence, Department of Neurology, Huashan Hospital, State Key Laboratory of Brain Function and Disorders and MOE Frontiers Center for Brain Science, Fudan University, Shanghai, China. [2]Key Laboratory of Computational Neuroscience and Brain-Inspired Intelligence (Fudan University), Ministry of Education, Shanghai, China. [3]School of Data Science, Fudan University, Shanghai, China. [4]Centre for Functional MRI of the Brain (FMRIB), Nuffield Department of Clinical Neurosciences, Wellcome Centre for Integrative Neuroimaging, University of Oxford, Oxford, UK. [5]Department of Computer Science, University of Warwick, Coventry, UK. [6]Department of Radiology, Shanghai Fourth People's Hospital Affiliated to Tongji University School of Medicine, Shanghai, China. [7]Fudan ISTBI—ZJNU Algorithm Centre for Brain-inspired Intelligence, Zhejiang Normal University, Jinhua, Zhejiang, China. [8]These authors contributed equally: Peng Ren, Wenjing Su, Jia You. ✉e-mail: hewang@fudan.edu.cn; jintai_yu@fudan.edu.cn; wcheng@fudan.edu.cn

(3) identify associated plasma biomarkers ($n = 313$, biochemistry, blood count and metabolic biomarker) and proteins ($n = 2920$); (4) discover modifiable factors and drug targets for intervention and treatment of organ-specific aging. This study highlights that imaging-based organ aging clocks offer a critical view for identifying individuals with accelerated aging, informing future risk of health problems, and promoting long-term health outcomes.

Results

Study population

The present study contains five research contents focusing on imaging-based biological age, as shown in the flow diagram of the study design in Fig. 1. The imaging-based aging clocks were first constructed based on 1777 IDPs (Supplementary Table 1) from a total of 11,000 healthy participants, with a median age of 61.0 years (interquartile range, 54.0–67.0), of whom 51.9% ($n = 5712$) were females and 98.0% ($n = 10,781$) were White ancestry. In particular, slightly different numbers of healthy participants were available for brain gray matter ($n = 5190$), brain white matter ($n = 4943$), heart ($n = 2818$), body composition ($n = 1739$), kidney ($n = 4379$), liver ($n = 3361$), pancreas ($n = 3595$) and eye ($n = 5397$). Details regarding the study populations are available in the "Methods" section and Supplementary Table 2.

Organ aging characterized by imaging

Leveraging a nested cross-validation framework[4], the LASSO regression estimated biological age for each organ, with the performance evaluated in the hold out test data. Comparable performance was observed between training and testing data, indicating no significant overfitting. The chronological age was predicted with varied accuracy for different organs (Fig. 2a). Specifically, high accuracy was achieved for brain gray matter (GM; $R = 0.81$, MAE = 3.61), brain white matter (WM; $R = 0.78$, MAE = 3.82), heart ($R = 0.72$, MAE = 4.11) and body composition ($R = 0.71$, MAE = 4.11). Meanwhile, relatively lower accuracy was achieved for kidney ($R = 0.34$, MAE = 5.84), liver ($R = 0.27$, MAE = 5.95), pancreas ($R = 0.29$, MAE = 5.95) and eye ($R = 0.27$, MAE = 6.53). Comparable prediction accuracy was observed for different sexes (Fig. 2b). Comparable performance was observed between training and testing data, indicating no significant overfitting (Supplementary Table 3). In sensitivity analyses, we found that the models demonstrated strong generalizability across different ancestries but weaker generalizability across different age bands (Supplementary Tables 4 and 5). This implies that training the organ-specific biological age models exclusively on a subsample may introduce bias. The models, trained on mid-to-late adulthood and White ancestry, may not fully capture early-life changes, potentially leading to less accurate estimation of age gaps and disease risk. Future work will benefit from external validation of these organ-specific aging clocks in cohorts with more diverse ancestral, demographic and clinical profiles.

The interrelationships between the age gap of different organs were estimated with SEM (Fig. 2c, d). Specifically, the heart and body composition exhibited the most extensive interrelationships with other organs. A 1-year increase in body composition age was associated with a 0.259-year increase in pancreas age, a 0.240-year increase in kidney age and a 0.063-year increase in heart age. For brain age, a 1-year increase in GM age was associated with a 0.515-year increase in WM age, a 0.137-year increase in heart and a 0.160-year increase in body composition. These association patterns remained consistent after regressing out chronological age, sex and imaging site (Supplementary Fig. 1).

Among all IDPs contributing to age modelling, IDPs related to the volume of grey matter were the most significant contributors to the biological age of brain grey matter. For the brain's white matter, the ICVF of white matter tracts contributed the most to biological age prediction. In the eye, the thickness of the ISOS-RPE layer was the key contributor to biological age, with opposing contributions observed in the central and inner subdivisions. The dynamic area of the ascending and descending aorta had the strongest influence on the age gap of the heart. In the liver and pancreas, volume contributed negatively to the age gap, while fat fraction and iron levels contributed positively. For the kidney, the parenchymal volume was negatively associated with the age gap (Fig. 3 and Supplementary Fig. 2).

Organ aging predicts the risk of disease and mortality

Cox proportional hazards models were employed to investigate the association between organ-specific age gap and risk of 12 broad categories of diseases (40 specific diseases) and all cause mortality (four cause-specific mortality), which were detailed in Supplementary Table 6. Generally, the greater the age gap, the higher the risk of the disease or mortality, indicated by a hazard ratio greater than 1 (Fig. 4a; Supplementary Figure 3 and Supplementary Table 7). Since organ-specific age gaps have already been transformed to z-score before survival analysis, i.e., SD = 1, the reported HR was already HR per SD of age gap. In other words, a 1-unit increase in the z-transformed age gap corresponds precisely to a 1-SD increase in the original age gap. The organ-specific age gap was most significantly associated with the diseases primarily targeting that organ (Fig. 4b). The age gap of brain GM showed the strongest association with the risk of dementia (HR = 1.81, SD = 5.46, 95% CI = [1.69, 1.93], $P_{FDR} = 1.62 \times 10^{-66}$, ΔC-index=0.06, $P = 3.26 \times 10^{-5}$) and mortality caused by nervous system (HR = 1.90, SD = 5.46, 95% CI = [1.62, 2.23], $P_{FDR} = 4.99 \times 10^{-13}$, ΔC-index=0.08, $P = 5.40 \times 10^{-3}$). The age gap of brain WM was most strongly associated with the risk of cerebrovascular diseases (HR = 1.46, SD = 6.67, 95% CI = [1.33, 1.60], $P_{FDR} = 4.99 \times 10^{-13}$, ΔC-index = 0.02, $P = 4.60 \times 10^{-3}$), dementia (HR = 1.99, SD = 6.67, 95% CI = [1.67, 2.38], $P_{FDR} = 1.08 \times 10^{-12}$, ΔC-index = 0.03, $P = 2.54 \times 10^{-3}$) and mental and behavioral disorders (HR = 1.25, SD = 6.12, 95% CI = [1.17, 1.34], $P_{FDR} = 3.22 \times 10^{-9}$, ΔC-index = 0.01, $P = 9.75 \times 10^{-3}$). In other words, a participant with 6.67 years increase (i.e., 1 SD) in brain GM age gap has almost 2-fold risk of incident dementia and 46% higher risk of incident cerebrovascular diseases. The age gap of the heart was most strongly linked to the risk of heart-related diseases, including hypertension (HR = 1.31, SD = 7.11, 95% CI = [1.22, 1.40], $P_{FDR} = 4.99 \times 10^{-13}$, ΔC-index = 0.01, $P = 6.17 \times 10^{-4}$), circulatory system disorders (HR = 1.21, SD = 7.03, 95% CI = [1.15, 1.28], $P_{FDR} = 6.51 \times 10^{-11}$, ΔC-index=0.01, $P = 4.24 \times 10^{-3}$) and arrhythmias (HR = 1.22, SD = 7.17, 95% CI = [1.13, 1.32], $P_{FDR} = 9.22 \times 10^{-6}$, ΔC-index = 0.004, $P = 0.10$). The age gap of the kidney was most strongly associated with renal failure (HR = 1.18, SD = 21.19, 95% CI = [1.13, 1.32], $P_{FDR} = 1.24 \times 10^{-5}$, ΔC-index = 0.004, $P = 0.02$). Moreover, the age gaps of the pancreas and eye were strongly associated with the risk of pancreas-specific disease, such as diabetes (HR = 1.20, SD = 23.65, 95% CI = [1.08, 1.34], $P_{FDR} = 0.00435$, ΔC-index=0.009, $P = 0.08$), and eye-specific disease, such as glaucoma (HR = 1.17, SD = 27.23, 95% CI = [1.10, 1.25], $P_{FDR} = 3.11 \times 10^{-5}$, ΔC-index=0.006, $P = 0.02$), respectively.

Meanwhile, the organ-specific age gaps also contributed to diseases not specific to the organs (Fig. 4a and Supplementary Table 7). Except for brain-specific disease, the age gap of the brain was also strongly associated with the risk of circulatory system disorder (HR = 1.14, SD = 5.33, 95% CI = [1.09, 1.19], $P_{FDR} = 2.03 \times 10^{-8}$, ΔC-index=0.004, $P = 3.58 \times 10^{-3}$). The age gap of the body composition was not only associated with osteoarthritis (HR = 1.13, SD = 6.77, 95% CI = [1.05, 1.23], $P_{FDR} = 0.01$, ΔC-index = 0.003, $P = 0.21$), but was also closely linked to the risk of peripheral artery diseases (HR = 1.32, SD = 6.81, 95% CI = [1.15, 1.53], $P_{FDR} = 8.45 \times 10^{-4}$, ΔC-index = 0.01, $P = 0.11$), mental and behavioral disorders (HR = 1.16, SD = 6.74, 95% CI = [1.05, 1.28], $P_{FDR} = 0.02$, ΔC-index = 0.006, $P = 0.21$). Besides, the mean age gap across the seven organs, which is the indicator of the overall health condition, was strongly associated with the risk of diseases across multiple categories of outcomes (Fig. 4c), such as dementia (HR = 1.62, 95% CI = [1.49, 1.76], $P_{FDR} = 1.61 \times 10^{-28}$, ΔC-index = 0.03, $P = 1.09 \times 10^{-3}$), renal failure (HR = 1.25, 95% CI = [1.19, 1.32], $P_{FDR} = 7.81 \times 10^{-16}$, ΔC-index = 0.008, $P = 7.43 \times 10^{-4}$), and all-cause mortality (HR = 1.23, 95% CI = [1.16, 1.31], $P_{FDR} = 1.15 \times 10^{-10}$, ΔC-index = 0.009, $P = 5.82 \times 10^{-4}$). In the two sensitivity analyses that removed the effects of chronological age, sex, and scanning site prior to survival analysis (Supplementary Table 8) and grouping organ-specific age gap into

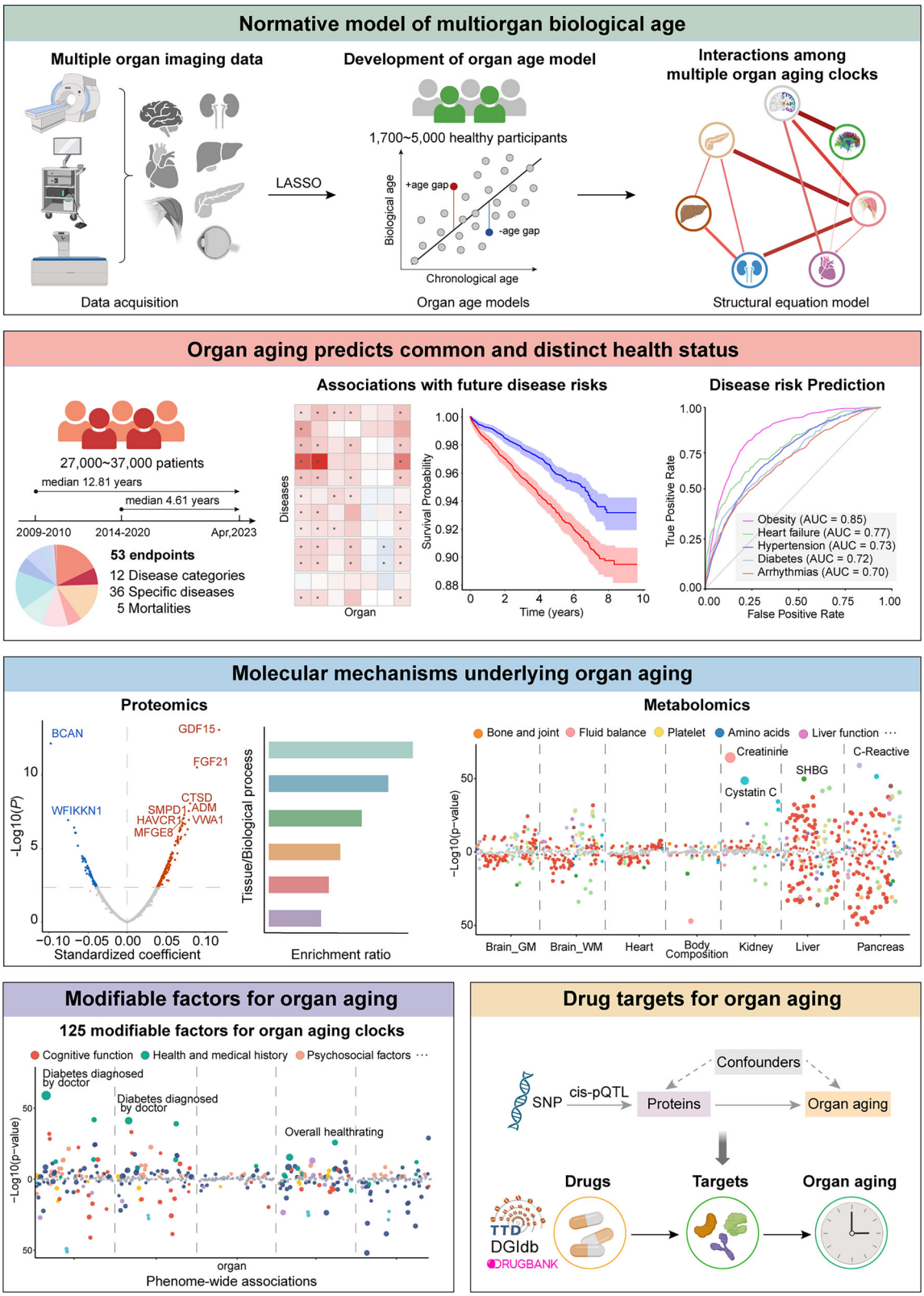

Fig. 1 | The overview of study design. a The biological age prediction models were constructed for seven different organs using imaging-derived phenotypes, along with pathway analysis on the relationships of age gaps across organs. **b** Examining whether organ-specific biological aging was associated with and predictive of future risk of the diseases primarily targeting the corresponding organ. **c** Identifying whether the proteins and blood biomarkers linked to organ aging exhibited organ-specific patterns. **d** The PheWAS analysis investigated whether organ aging is associated with organ-specific modifiable factors. **e** Identifying drug targets for the aging of the corresponding organs. Icons were created with BioRender.com.

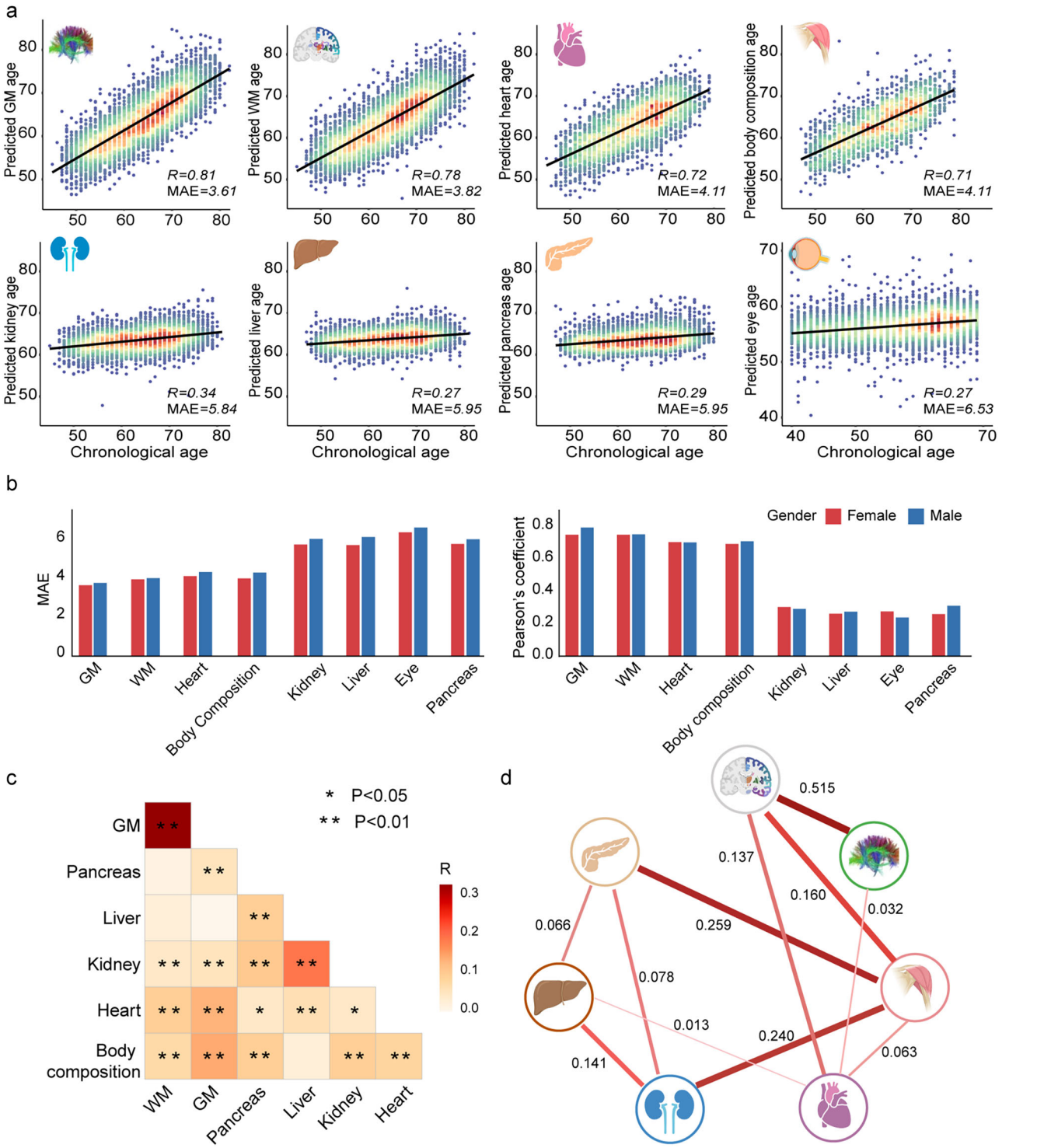

Fig. 2 | The performance of multi-organ aging models. a The scatter plot demonstrates the association between the chronological and predicted age of the eight different organs. The black solid lines denote the best-fit models. Pearson's coefficient (*R*) and mean squared error (MAE) were selected to measure the performance of organ age prediction models. **b** Similar to that of a, but stratified by sex to examine the potential sex difference of organ age prediction models. Different sexes are shown in different colors. **c** The organ age gap was defined as the difference between predicted and chronological age. Pearson's coefficients of associations between the age gap of different organs are shown, with darker representing higher relationships, *<0.05, **<0.01. **d** The multi-organ aging networks characterize statistical associations between the age gap of one organ and that of another. Significant links were inferred by SEM at a threshold of Bonferroni-corrected $P < (0.05/11$ pairs), thicker and darker lines represent stronger influences.

quartiles (Supplementary Fig. 4 and Supplementary Table 9), the direction and effect size of the associations between age gap and diseases remained largely the same. Moreover, in the sensitivity analysis that explicitly distinguishing confirmatory from exploratory results, we found that 24 out of the 32 significant associations ($P_{FDR} < 0.05$) in original results survived in confirmatory analysis, and 134 out of 181 significant associations ($P_{FDR} < 0.05$) in original results remained significant, indicating a more stringent control of multiple testing (Supplementary Tables 10 and 11). By

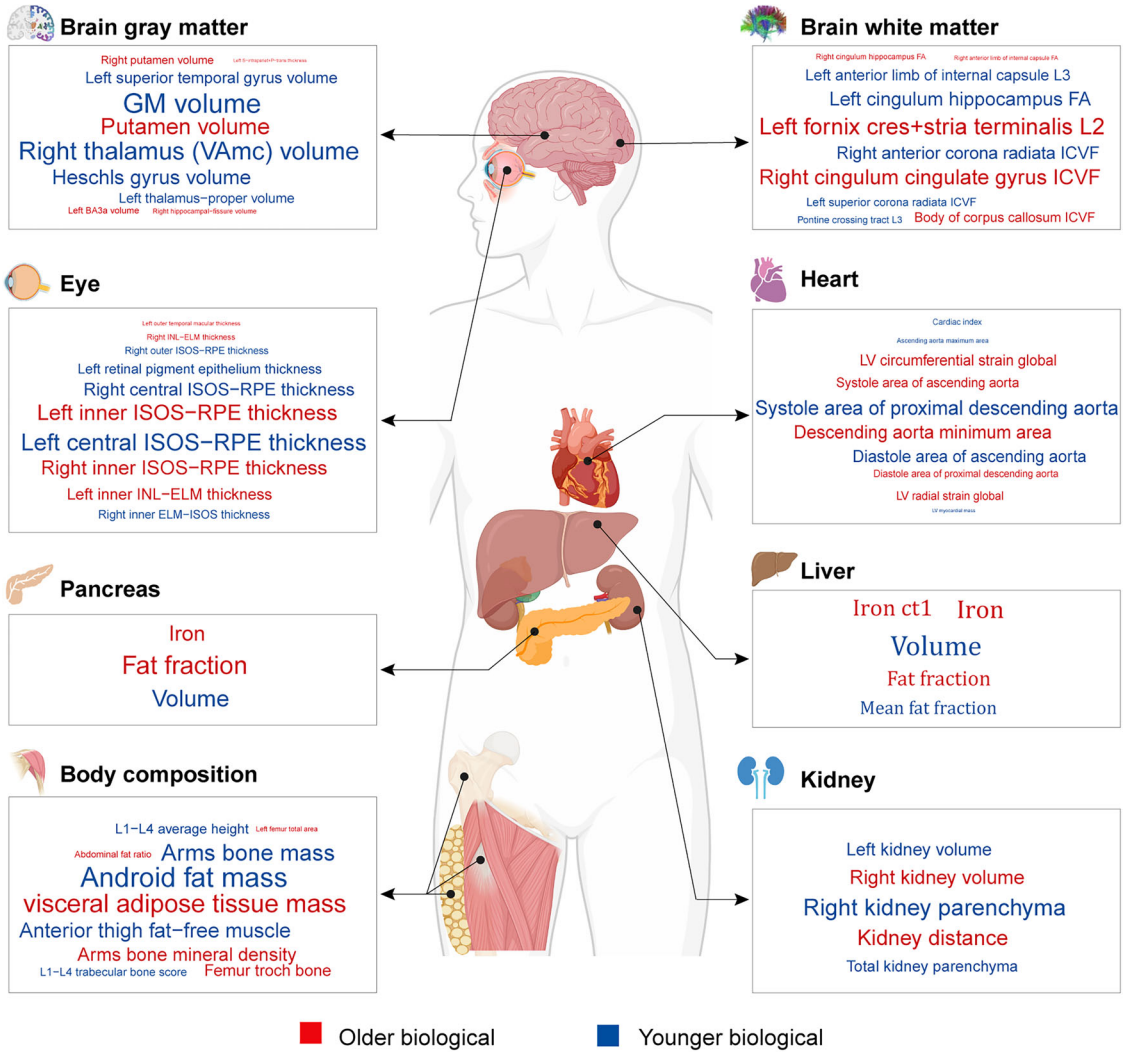

Fig. 3 | Feature interpretation of multiorgan age prediction models. The word cloud plot shows the weight of the top ten imaging features that contributed most to the optimal organ aging prediction models. The font sizes are proportional to the absolute weight values, with positive weights rendered in red and negative weights rendered in blue. The image was created with BioRender.com.

comparing the HR estimates between high-accuracy and low-accuracy aging clocks, we found that low-accuracy aging clocks showed lower risk (HR) of incident disease ($T = -9.11$, $P = 5.16 \times 10^{-18}$) than high-accuracy aging clocks, which may come from the sparse and limited number of imaging features currently available for these organs.

The prediction analysis assessed whether organ-specific biological age (BA) could predict the incident of disease and mortality beyond the effect of chronological age (CA). We established LightGBM prediction models with IDPs contributing most to biological organ age and compared these models to the baseline model that included only chronological age and sex. We observed that, by incorporating information from all organs except the eye, the prediction model outperformed the baseline model for various diseases (Supplementary Fig. 5 and Supplementary Table 12), including obesity ($AUC_{BA} = 0.78$, $AUC_{CA} = 0.54$), dementia ($AUC_{BA} = 0.80$, $AUC_{CA} = 0.73$), heart failure ($AUC_{BA} = 0.75$, $AUC_{CA} = 0.72$), diabetes ($AUC_{BA} = 0.71$, $AUC_{CA} = 0.59$), as well as for all-cause mortality ($AUC_{BA} = 0.71$, $AUC_{CA} = 0.70$). Furthermore, for many organ-specific diseases and mortality, the prediction models incorporating information about organ-specific biological age also demonstrated superior performance compared to the baseline model (Fig. 4d; Supplementary Fig. 5 and Supplementary Table 12). Specifically, the model based on GM age outperformed the baseline model for dementia ($AUC_{BA} = 0.82$, $AUC_{CA} = 0.71$), the model incorporating heart age surpassed the baseline model for heart failure ($AUC_{BA} = 0.78$, $AUC_{CA} = 0.71$) and hypertension ($AUC_{BA} = 0.74$, $AUC_{CA} = 0.64$), the model based on body composition age exceeded the baseline model for obesity ($AUC_{BA} = 0.86$, $AUC_{CA} = 0.52$). We further conducted a sensitivity analysis that split 70% of the data as training data and the resting 30% data as hold-out test set. Consistent patterns of prediction to that of 10-fold cross-validation were observed (Supplementary Fig. 5 and Supplementary Table 13).

Association between organ aging and blood biomarkers

In considering the frequent substance exchange between blood and organs, we further identified 1198 significant associations between the age gap of seven organs and 299 blood biochemistry, blood count and metabolic biomarkers in participants with available organ-specific data (brain GM, $N = 25{,}241$; brain WM, $N = 23{,}617$; heart, $N = 14{,}112$; kidney, $N = 20{,}218$; body composition, $N = 8975$; liver, $N = 14{,}420$; pancreas, $N = 15{,}892$; Supplementary Tables 14–16). Overall, the highest number of significant associations was observed between blood biomarkers and the age gap of liver (247), followed by pancreas (245), brain GM (198), brain WM (196), kidney (128), heart (127), and body composition (57) ($P_{FDR} < 0.05$). Meanwhile, 290 out of 299 blood biomarkers were associated with at least two organs, and the associations were dominant by lipoprotein and lipid and fatty acids across seven organs. In particular, leukocyte count was the biomarker that

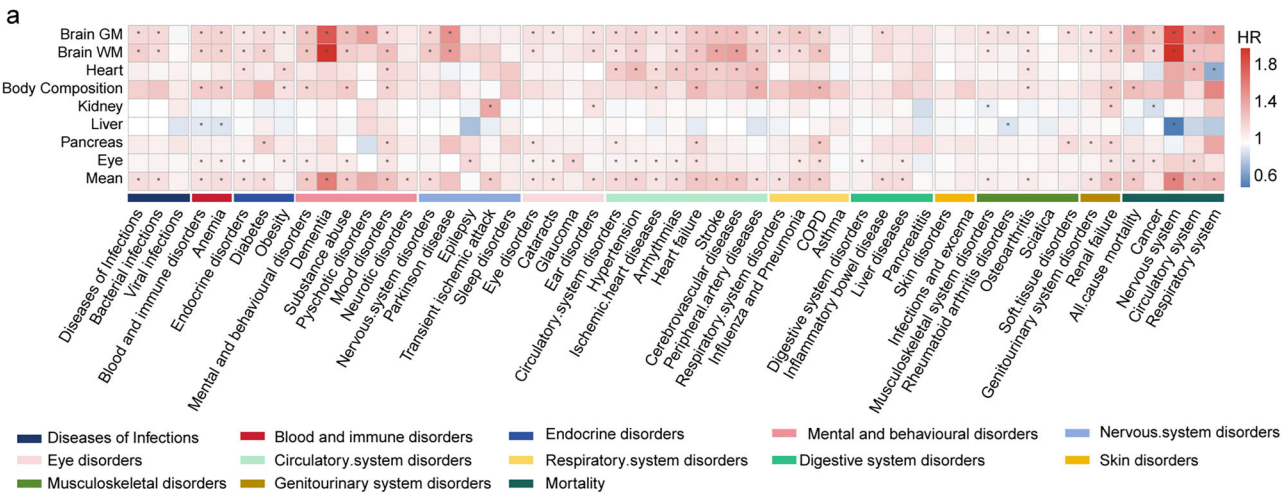

b

Organ	Diseases	HR (95% CI)
Brain GM	Dementia	1.81 (1.69 to 1.93)
	All−cause mortality	1.37 (1.29 to 1.47)
	Nervous system mortality	1.90 (1.62 to 2.23)
Brain WM	Cerebrovascular diseases	1.46 (1.33 to 1.60)
	Dementia	1.99 (1.67 to 2.38)
	Mental and behavioural disorders	1.25 (1.17 to 1.34)
Heart	Hypertension	1.31 (1.22 to 1.40)
	Circulatory system disorders	1.21 (1.15 to 1.28)
	Arrhythmias	1.22 (1.13 to 1.32)
Body Composition	Substance abuse	1.33 (1.15 to 1.54)
	Peripheral artery diseases	1.32 (1.15 to 1.53)
	Heart failure	1.34 (1.15 to 1.56)
Kidney	Renal failure	1.18 (1.11 to 1.26)
	Transient ischemic attack	1.40 (1.17 to 1.68)
	Cancer mortality	0.88 (0.81 to 0.96)
Liver	Leukaemia	0.67 (0.52 to 0.86)
	Nervous system mortality	0.49 (0.29 to 0.83)
	Rheumatoid arthritis disorders	0.89 (0.81 to 0.97)
Pancreas	Renal failure	1.16 (1.08 to 1.24)
	COPD	1.23 (1.10 to 1.38)
	Soft tissue disorders	1.14 (1.06 to 1.23)
	Eye disorders	1.09 (1.04 to 1.15)
	Diabetes	1.20 (1.08 to 1.34)
Eye	All−cause mortality	1.13 (1.09 to 1.17)
	COPD	1.13 (1.07 to 1.18)
	Glaucoma	1.17 (1.10 to 1.25)

c

Diseases	HR (95% CI)
Dementia	1.62 (1.49 to 1.76)
Renal failure	1.25 (1.19 to 1.32)
Mental and behavioural disorders	1.24 (1.17 to 1.30)
Circulatory system disorders	1.16 (1.11 to 1.20)
Hypertension	1.19 (1.13 to 1.24)
All−cause mortality	1.23 (1.16 to 1.31)
Cerebrovascular diseases	1.26 (1.17 to 1.35)
Influenza and Pneumonia	1.21 (1.14 to 1.29)
Mood disorders	1.28 (1.18 to 1.39)
Heart failure	1.26 (1.16 to 1.36)
Endocrine disorders	1.11 (1.07 to 1.15)
Nervous system disorders	1.15 (1.09 to 1.21)
Arrhythmias	1.15 (1.09 to 1.22)
Genitourinary system disorders	1.12 (1.07 to 1.17)
Substance abuse	1.23 (1.13 to 1.34)
Cataracts	1.11 (1.06 to 1.16)
Eye disorders	1.11 (1.06 to 1.15)
COPD	1.22 (1.12 to 1.33)
Anemia	1.14 (1.07 to 1.20)
Nervous system mortality	1.60 (1.29 to 1.97)
Stroke	1.23 (1.12 to 1.35)
Diseases of Infections	1.14 (1.07 to 1.21)
Circulatory system mortality	1.29 (1.14 to 1.46)
Respiratory system disorders	1.12 (1.06 to 1.18)
Blood and immune disorders	1.11 (1.06 to 1.17)
Bacterial infections	1.13 (1.06 to 1.20)

d

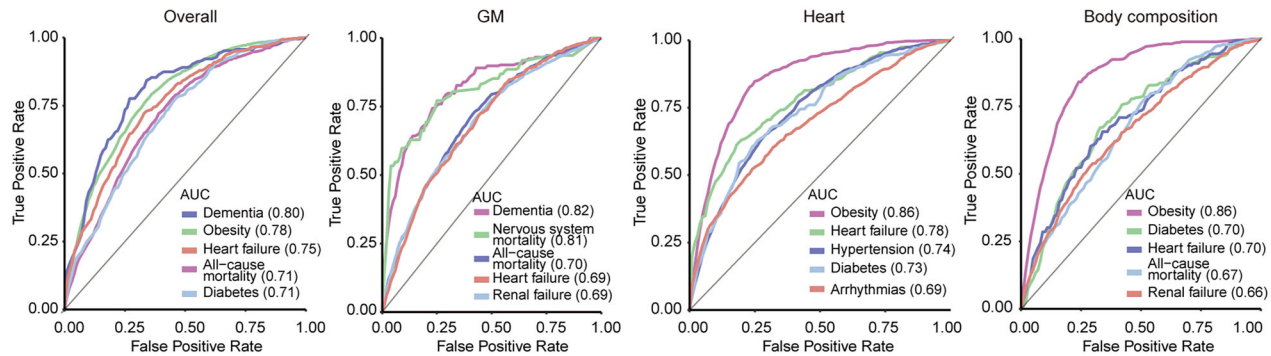

Fig. 4 | Organ age gap influenced the risk of diseases and mortality. a The heatmap demonstrates the association between the organ-specific age gaps (y-axis) and the risk of 13 different categories of diseases or health outcomes (x-axis). The hazard ratio (HR) values are color-coded, with warm colors representing positive associations between organ age gap and disease risk, and cool colors representing negative associations. The FDR correction was applied across all possible organ-disease pairs, with those associations with FDR-corrected $P < 0.05$ considered significant and marked with an asterisk. The association between the average age gap across organs and disease risk is also demonstrated in the last row of the heatmap. **b** Each organ's most significant associations are shown with a forest plot for clarity. **c** The association between the mean age gap across organs and disease risk is also plotted in a form of forest plot. **d** The prediction of the incident diseases and mortality during the entire visit was made using information reflecting biological age, with IDPs contributing most (top 50%) to the biological age of organs selected as predictors. The performance was evaluated with average AUC across 10-folds. Here we separately illustrated the top predictions with the largest AUC using information reflecting biological age of all organs, as well as GM, heart and body composition.

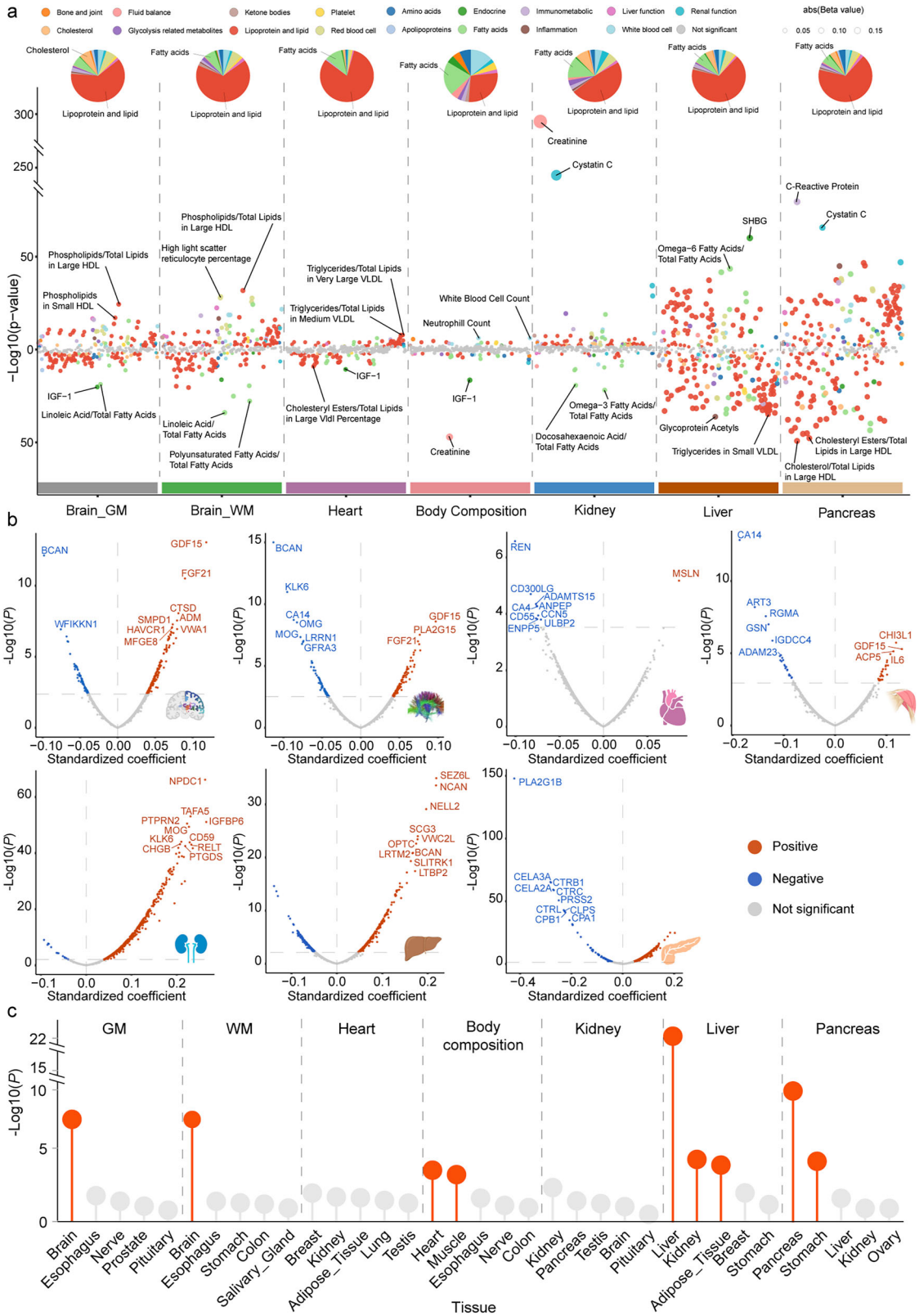

showed the highest total number of significant positive associations (six organs), and omega-3 fatty acids to total fatty acids percentage, IGF-1 was the biomarker that exhibited the highest total number of significant negative associations (six organs).

Among the associated blood biomarkers, several biomarkers exhibited organ-specific associations (Fig. 5a): creatinine, the waste product made by muscle and cleared by kidney[11], was the biomarker with the most significant negative association (standardized beta = −0.19, $P_{FDR} = 1.90 \times 10^{-45}$) with the age gap of body composition and the most significant positive association (standardized beta = 0.31, $P_{FDR} = 4.76 \times 10^{-292}$) with the age gap of the kidney. Cystatin C, a sensitive marker for assessing kidney function[12], also exhibited a strong positive association (standardized beta = 0.25,

Fig. 5 | Association between plasma signature and multi-organ age. a The scatter plot demonstrates the association between organ-specific age gap and blood biomarkers. The blood biomarkers were classified into 17 different categories and color-coded. The *x*-axis represents seven different organs, and the y-axis represents the −log10 transformation of uncorrected *P* value from the associations between organ age gaps and concentration of biomarkers. The FDR was applied across all 310 × 7 blood biomarker-organ pairs, and the associations with FDR-corrected $P < 0.05$ were considered significant and shown in color. The non-significant associations are shown in grey. The size of points is proportional to the absolute of beta values. The positive associations are shown above $y = 0$, and the negative associations are shown below $y = 0$. The two most significant positive associations and negative associations are labelled. The distributions of significantly associated blood biomarkers across categories are shown in pie charts, with the two most widely distributed categories labeled. **b** The volcano plot shows the association between organ age gap and protein concentrations. The *x*-axis represents the standardized coefficient of the association, and *y*-axis represents the -log10 transformation of the uncorrected *P* value. The FDR correction was applied across all 2920 × 7 protein-organ pairs, and the significance was determined by FDR-corrected $P < 0.05$. The significant positive associations are shown in red, and the negative associations are in blue. The dashed horizontal grey lines denote FDR-corrected $P = 0.05$, and non-significant associations are shown in grey. The top ten associations are annotated. **c** The lollipop plot demonstrates the enrichment of the proteins associated with organ-specific age gaps in different tissues. The tissue-enriched gene sets are priori defined by GTEx. The x-axis represents the top five tissues in enrichment results of the seven organs, and the y-axis represents the −log10 transformation of the uncorrected *P* values. The significance was determined by FDR-corrected $P < 0.05$ for each organ, and the significantly enriched tissues are shown in red color. The non-significant enrichments are shown in grey.

$P_{FDR} = 1.59 \times 10^{-244}$) with the age gap of the kidney. The higher ratio of triglycerides and total lipids in very large very-low-density lipoprotein (VLDL), which reflects the predominance of triglycerides in VLDL and has been linked to the risk of cardiovascular disease (e.g., atherosclerosis)[13,14], showed a positive association with the age gap of the heart (standardized beta = 0.05, $P_{FDR} = 6.49 \times 10^{-8}$).

Consistent relationships were identified between organ age gaps and blood biomarkers with scanning site included as an additional covariate (Supplementary Table 17). By comparing the absolute beta estimates between high-accuracy and low-accuracy aging clocks, we found that low-accuracy aging clocks showed stronger absolute effect size (beta) for associations with metabolites (T = 3.60, $P = 3.60 \times 10^{-63}$).

Association between organ aging and proteomic signatures

The associations between 2920 plasma proteins and the age gap of seven organs were characterized using general linear models in participants with available proteomic and organ-specific data (brain GM, $N = 5525$; brain WM, $N = 5219$; heart, $N = 2878$; kidney, $N = 4417$; body composition, $N = 1673$; liver, $N = 3392$; pancreas, $N = 3608$; Supplementary Table 18). Overall, 2230 significant associations were found between seven organs and 1174 proteins. Specifically, the highest number of associations were observed for the pancreas (627) and kidney (620), followed by the liver (367), GM (249), WM (222). Meanwhile, 676 out of 1174 proteins were identified in at least two organs. CXCL17, FGF21, and LAMP3 were the proteins with the highest total number of significant positive associations (six organs), and CA14, CD93, and GSN were the proteins with the highest total number of significant negative associations (four organs).

However, we discovered obvious heterogeneity in the proteins exhibiting the most significant associations (Fig. 5b and Supplementary Table 19). Specifically, for the brain, BCAN and GDF15 showed the most significant negative and positive association with both the age gap of GM and WM systems. PLA2G1B and CELA3A, secreted specifically by the pancreatic cells, were the proteins with the most significant negative association with the age gap of the pancreas. ADAMTS15, expressed during early cardiac development, was among the proteins showing the most significant negative association with the age gap of the heart. Consistent relationships were identified between organ age gaps and protein concentration with scanning site as an additional covariate (Supplementary Table 20).

In tissue enrichment analysis, for most organs, the proteins with negative associations were significantly enriched in the over-expressed genes of the corresponding organ (Fig. 5c and Supplementary Table 21). In particular, the proteins exhibited negative association with GM ($P_{FDR} = 3.26 \times 10^{-6}$) and WM ($P_{FDR} = 3.30 \times 10^{-6}$) were enriched in over-expressed genes of brain tissue. This organ-specific pattern was also observed for body composition ($P_{FDR} = 0.02$), liver ($P_{FDR} = 2.16 \times 10^{-21}$), and pancreas ($P_{FDR} = 7.41 \times 10^{-13}$).

Similarly, in GO biological process enrichment, the proteins exhibiting negative associations were significantly enriched in the biological processes associated with the corresponding organ (Supplementary Fig. 6 and Supplementary Table 22). In particular, we observed enrichment in axons and synapses for brain aging, phenol−containing compound metabolic process ($P_{FDR} = 0.006$) and regulation of prostaglandin−E synthase activity ($P_{FDR} = 0.006$) for kidney aging, fibrin clot formation of blood coagulation ($P_{FDR} = 0.009$) and intrinsic pathway of blood coagulation ($P_{FDR} = 0.009$) for liver, digestion ($P_{FDR} = 0.012$) for pancreas. On the contrary, for most organs, the proteins with positive associations were significantly enriched in immune-related processes (Supplementary Table 22), such as defense response to gram-negative bacterium and inflammatory response. By comparing the absolute beta estimates between high-accuracy and low-accuracy aging clocks, we found that low-accuracy aging clocks showed a stronger absolute effect size (beta) for associations with plasma proteomic levels ($T = 27.01$, $P = 5.95 \times 10^{-156}$).

Modifiable factors for organ aging

In PheWAS analysis, we investigated the associations between organ-specific age gaps and 143 modifiable factors, with the number of eligible participants ranging from 2416 to 41871. Overall, obvious diversities in the number of significant associations were identified for GM ($n = 91$), WM ($n = 67$), heart ($n = 23$), body composition ($n = 63$), kidney ($n = 50$), liver ($n = 85$) and pancreas ($n = 86$). Among all the significant associations, 6 early life and family history factors, 59 lifestyle and environmental factors, 14 cognitive functions, 11 health and medical history, 2 physical measures, 27 psychosocial factors and 6 sociodemographic factors were associated with the age gap of organs (Supplementary Table 23).

Among all the examined factors, 114 out of 143 factors contributed to the age gaps of multiple organs (Fig. 6a). Specifically, longer time spent watching television, more alcohol usually taken with meals, more pack-years of smoking, and worse overall health rating were associated with accelerated aging of almost all organs, while more cereal intake, stronger hand grip strength, and higher number of days/weeks of moderate physical activity (10+ minutes) were among the factors that associated with decelerated aging of most organs.

Meanwhile, organ-specific association patterns were also observed for age gaps. In particular, compared to other factors, cognitive functions were more associated with the age gap of brain systems. Similarly, the number of days/weeks of physical activity was clearly more associated with the age gap of body composition and the pancreas. Besides, in the analysis that included eye (Supplementary Fig. 7 and Supplementary Table 24), the factor with the most significant association was maternal smoking around birth (standardized beta = 0.15, $P_{FDR} = 2.86 \times 10^{-36}$). Meanwhile, longer time spent watching television was also among the factors exhibiting the most significant associations with the aging of the eye (standardized beta = 0.05, $P_{FDR} = 1.85 \times 10^{-7}$).

Prioritized drug targets for organ aging

We further employed cis-MR analysis to pinpoint potential drug targets with potential for pharmacological intervention in regulating organ aging. For the 15 cis-MR relationships between plasma proteins and organ-specific

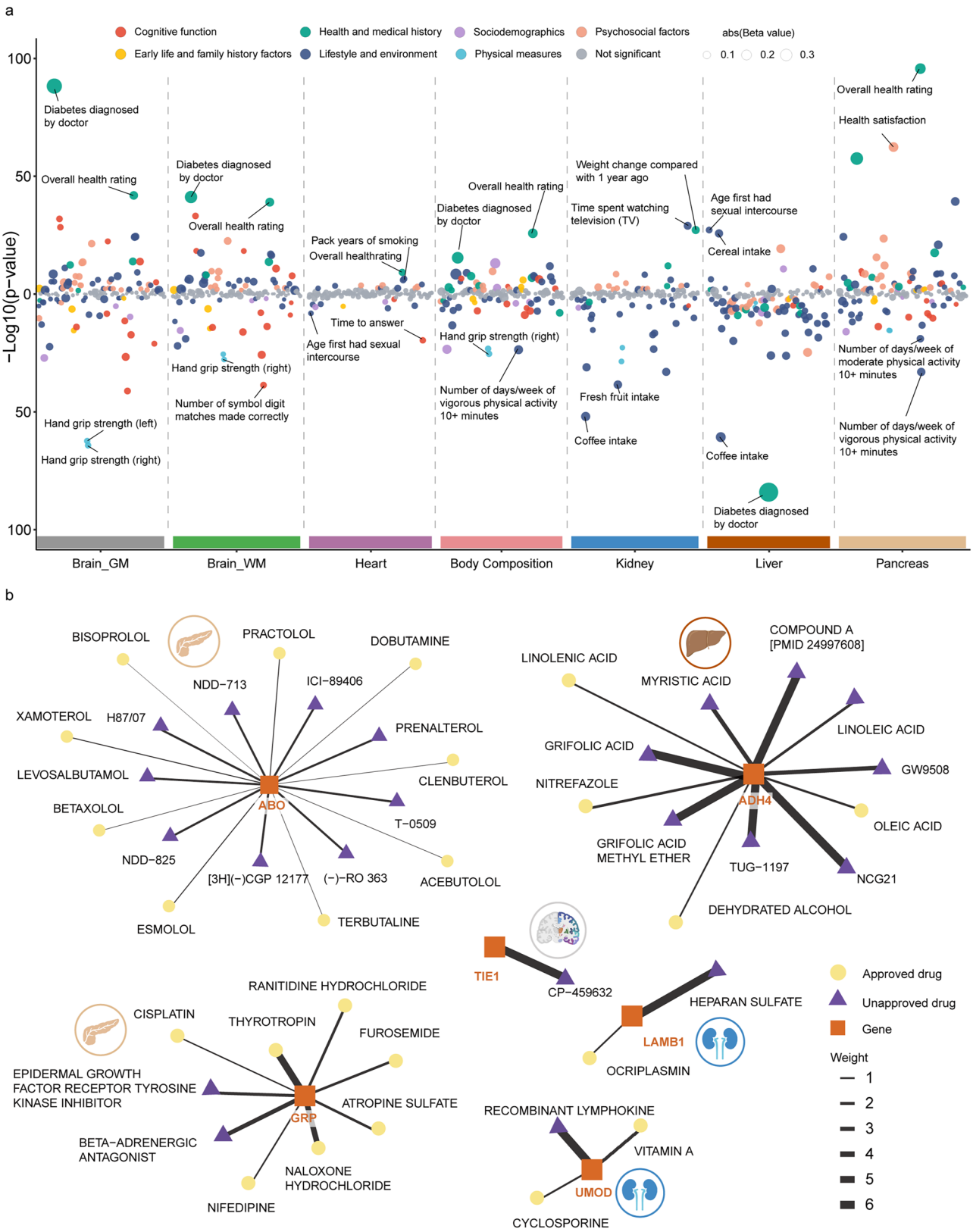

aging and 2 cis-MR relationship between CSF protein and organ-specific aging, most of them were robustly supported by at least three MR methods. We did not observe significant horizontal and directional pleiotropy (all $P_{FDR} > 0.05$) for the significant cis-MR relationships (Supplementary Table 25). A total of 14 plasma proteins were identified to have significant causal relationships with organ aging (FDR-corrected $P < 0.05$, Supplementary Table 25). Among them, CHRDL2, ITIH4, LRRC37A2, SEMA3F, and TIE1 proteins were causally associated with brain aging, with the TIE1 protein further confirmed using cerebrospinal fluid. Transcriptomic analyses of human brain microvessels have shown that genes associated with

Fig. 6 | Modifiable factors and drug targets for organ age gaps. a The scatter plot demonstrates the association between organ-specific age gap of the eight different organs and the factors at the imaging visit, with the FDR applied across all 143 × 7 factor-organ pairs, and only those associations with FDR-corrected $P < 0.05$ were considered significant. This study assessed seven categories of factors: socio-demographics, cognitive function, lifestyle and environment, early life and family history factors, physical measures, psychosocial factors, and health and medical history. The significant associations of different categories of factors are drawn in different colors, and the non-significant associations are shown in grey. The size of points is proportional to the absolute of beta values. The *x*-axis represents the eight different organs and the *y*-axis represents the −log10 transformation of the uncorrected *P* values of the association between organ age gap and factors. The positive associations are shown above $y = 0$, and the negative associations are shown below $y = 0$. The two most significant positive associations and negative associations are labeled. **b** The drug-target network showed the approved and unapproved drugs for the targets that were identified by cis-MR between plasma/cerebrospinal fluid proteins and imaging-based organ age gap. The wider the line, the stronger the evidence observed between the drug and target.

endothelial senescence and adhesion, including TIE1, are upregulated in association with elevated tau pathology, indicating a link between TIE1 expression and cerebrovascular changes in age-related neurodegenerative disease[15]. ABO, CLPS and GRP proteins were causally associated with pancreatic aging, where CLPS is a cofactor needed by pancreatic lipase for efficient dietary lipid hydrolysis. GRP and its receptor are endogenously expressed in normal human pancreatic tissue, indicating a role in local pancreatic signaling[16]. Beyond its physiological functions, circulating GRP levels have been reported to be associated with altered glucose metabolism and increased pro-inflammatory cytokines following pancreatitis. These features—metabolic dysregulation, chronic inflammatory signaling, and disrupted endocrine–paracrine communication—are hallmarks of age-related pancreatic functional decline[17]. ERI1, MSRA, and SPINK8 were causally associated with eye aging, among which MSRA is an enzyme that protects cells in the retina and lens from oxidative stress[18]. LAMB1 and UMOD were causally associated with kidney aging, where *UMOD* encodes for uromodulin, the most abundant protein excreted in normal urine[19]. Common noncoding variants in the UMOD promoter have been associated with increased susceptibility to chronic kidney disease and age-dependent renal lesions in experimental models, supporting a genetic basis for UMOD's role in kidney aging–related pathology[20]. Proteomic analyses of kidney aging and disease have shown that alterations in basement membrane composition, including changes in laminin chains (e.g., LAMB1), are a consistent feature of aging and progressive renal pathology[21]. Six proteins —ADH4, LAMB1, ABO, GRP, UMOD, and TIE1—are either approved drug targets or currently under investigation in clinical trials, as documented in DrugBank, the Therapeutic Target Database and the Drug–Gene Interaction Database (Fig. 6b). Notably, the MR-identified proteins represent candidate drug targets associated with organ aging. These findings are hypothesis-generating and require functional follow-up, including in vitro/in vivo experiments, tissue-specific knockdown/overexpression studies, and ideally interventional trials to validate therapeutic potential.

Discussion

Our research represents the first comprehensive examination of imaging-based aging clocks across seven organs, utilizing 1777 organ-specific IDPs derived from 11,000 healthy individuals in the UKB. Findings in this study demonstrate that imaging-based biological organ aging exhibited distinct organ-specific patterns. Specifically, selective interrelationships were identified across organs, among which the heart and body composition exhibited the most extensive interrelationships compared to other organs. Organ-specific biological aging could influence and predict incident diseases and mortality, primarily affecting the corresponding organ, achieving AUCs > 0.8 for dementia and obesity. Meanwhile, 966 shared and 507 organ-specific molecular signatures were identified for the biological aging of different organs. Distinct modifiable factors were discovered for various organs, where cognitive functions were more closely associated with the brain and physical activities were more related to body composition. Moreover, 14 potential drug targets were identified for the intervention of organ-specific aging. Altogether, our novel imaging-based aging clocks provide alternative approaches to advance the current understanding of human aging and inspire targeted interventions to mitigate organ-specific disease risks.

In contrast to existing plasma proteomic[4,5,22], metabolic[2,23], epigenetic[24], and facial[25] aging clocks, which rely on empirical knowledge or external sources of in vitro data to estimate organ aging, our imaging-based aging clocks demonstrate the advantage of higher organ specificity and reduced reliance on manual selection. Meanwhile, compared to in vitro cell aging estimated at single-cell resolution[26], in vivo imaging provides a compromise between specificity and feasibility, such that imaging-based modeling enables a more objective, specific, and practical estimation of organ age. Furthermore, although we did not introduce any information about organ-enriched proteins when constructing age prediction models, we found that the proteins and blood biomarkers associated with imaging-defined organ age exhibited organ-specific patterns, which highlights that our models were not only organ-specific at the macro scale, as demonstrated through imaging, but also at the micro scale. This dual-level specificity underscores the robustness of the imaging-based approach in capturing organ-specific biological aging processes.

Earlier investigations have either introduced bias when attempting to infer the directionality of associations or have separately characterized multiorgan aging network structures within body systems and brain systems[27]. By leveraging UKB imaging data of the brain and other organs collected from the same imaging visit, this study offers a complementary view of how the aging processes of the brain and other organs may influence one another. In particular, we discovered the selective association between the aging of the brain and that of the heart and body composition. The observed statistical association between brain and heart age gaps is consistent with a hypothesized brain–heart connection, given that the brain regulates cardiac activity via the sympathetic and parasympathetic branches of the autonomic nervous system[27], and that mental disorders, such as posttraumatic stress disorder, have been associated with an increased risk (HR = 1.61) of coronary heart disease[28]. The findings of this study, together with previous research[4], contribute to an emerging landscape of statistically inferred multiorgan aging networks. Notably, in contrast to the MR analysis that provided causal insights, the SEM analyses serve a complementary, exploratory role by describing patterns of association among organ-specific age gaps that are compatible with certain network structures rather than establishing causality.

While previous investigations have implied the organ-specific pattern of the association between fluid-based aging and diseases[4,5], there is a lack of systematic assessment of how organ-specific aging contributes to incident diseases. Compared with prior reports, our findings revealed more organ-specific patterns for brain and heart, refined the previous understanding of the relationship from kidney-to-metabolic disease to a more specific kidney-to-renal failure connection. Additionally, we extended the organ-specific patterns to the pancreas and eye by demonstrating their predictive capacity for the risk of incident diabetes and glaucoma. For most diseases, our imaging-based aging clocks showed a generally larger hazard ratio than the previous single proteomic aging clock (HR < 1.2 for all diseases) in UKB[22]. Previously established organ-specific proteomic aging clocks showed a higher risk of heart failure (heart age: HR = 2.37) and mortality (all proteins: HR = 1.54) in the LonGenity cohort[5] and higher risk of kidney failure in UKB-PPP cohort[6]. However, given the potential systematic difference between cohorts, e.g., incidence rate, demographic profiles, careful consideration is needed before comparison. Moreover, by estimating the mean age gap across all organs, we demonstrated that this simple proxy for individual aging predicted the risk of incident diseases affecting multiple organs and outperformed the single proteomic aging clock (HR < 1.2 for all

diseases)[22]. By monitoring this biomarker, healthcare providers could detect early signs of multiorgan dysfunction and implement preventive strategies to mitigate the overall deterioration of health. Even more, we found that IDP information related to organ biological age could predict the incident of diseases and mortality beyond that of chronological age and sex, further highlighting the potential of imaging-based biological age in informing abnormality in the aging process. Compared to existing simple dementia risk prediction models (CAIDE[29], DRS[30], and ANU-ADRI[31]), which are limited by reliance on potentially biased self-reported and clinical variables, our imaging-based risk prediction model not only achieves superior predictive performance but also outperforms in objectivity and biological relevance, representing a more robust tool for early dementia risk assessment.

As previously reported, the liver[32], kidney[33], and pancreas[34] are vital organs in regulating metabolism. Accordingly, we found that these three organs—liver, kidney, and pancreas exhibited the highest number of significant associations with both blood biomarkers and plasma proteins. Moreover, we demonstrated that the proteins and blood biomarkers showing the most significant associations with organ age exhibited clear organ-specific patterns. Among these, plasma GDF15[35], the protein exhibiting the strongest positive association with accelerated brain aging, emerges as the strongest predictor of incident vascular dementia[36]. Higher levels of creatinine and cystatin C were associated with accelerated kidney aging, with both being the most widely used clinical measure of kidney function[37]. Meanwhile, for most organs, higher expression of proteins related to immune response was associated with accelerating organ aging, recapturing that low-grade and chronic damage resulting from increased inflammation levels is a hallmark of aging[38,39]. Altogether, these findings collectively illustrate the organ-specific characteristics of imaging-based age from a microscale perspective. Further assessment of these organ aging-related biomarkers holds the potential for inspiring new targets for effective prevention and intervention of aging.

Although the aging clocks for certain organs (e.g., kidney, liver, pancreas) demonstrated only moderate predictive performance, they may still provide valuable insights into organ-specific aging processes. This is supported by: (1) Despite their lower performance in predicting age, the aging of these organs did exhibit stronger hazard ratios for their organ-specific diseases than most of the other diseases, indicating an organ-specificity at the macro scale. For instance, aging of the pancreas exhibited a stronger risk for diabetes, aging of the glaucoma showed stronger risk for eye and aging of the kidney exhibited stronger risk for renal failure; (2) Strong associations were observed between accelerated aging in these organs and clinically validated organ-specific plasma biomarkers that reflect their functional status, further implying an organ-specificity at micro scales. For instance, creatinine and cystatin C exhibited the strongest positive association with kidney aging, and SHBG showed the strongest association with the aging of the liver. (3) A previous pancreas aging clock based on raw abdominal MRI and deep learning achieved higher performance (MAE = 2.94 ± 0.03) but lower organ-specificity than ours, which is in line with the recent advocation for a balanced consideration of both model performance and clinical relevance[10]. Altogether, we found that the low-accuracy aging clocks do capture organ-specific patterns at both macro and micro scales. While future improvement in model performance is crucial for these lower-performing organs, they exhibit meaningful organ-specific patterns and are informative of the aging and health status of the corresponding organs.

Several issues should be considered when interpreting our findings. First, although we leveraged a large set of multimodal imaging-derived phenotypes, the available IDPs for some organs—particularly the kidney, liver and pancreas—remain relatively coarse, which may limit the precision of organ-specific aging estimates. Second, the study population was drawn from the UK Biobank imaging cohort and consisted predominantly of White European individuals aged 40–96 years. As a result, the proposed imaging-based aging clocks primarily capture later-life aging patterns and may not fully generalize to younger populations. While external validation in an independent cohort was unfortunately not feasible within the current study scope due to limited availability of comparable multimodal and multiorgan datasets, future work will benefit from external validation of these organ-specific aging clocks in independent cohorts with more diverse ancestral, demographic and clinical profiles, to further assess their generalizability and translational potential. Third, most organs were imaged only once for the majority of participants, such that the derived organ-specific age gaps represent cross-sectional deviations from normative aging rather than within-individual longitudinal change, precluding direct modeling of aging rates or temporal dynamics. Finally, although we adjusted for a broad range of demographic, lifestyle and socioeconomic covariates, residual confounding—such as from comorbidities or medication use—cannot be fully excluded, and the observed associations should be further validated.

This study represents the first comprehensive evaluation of organ-specific aging clocks based on multimodal imaging. The imaging-based aging clocks established in this study not only exhibit organ specificity at both macro and micro scales but are also highly predictive of incident diseases that affect the corresponding organs, highlighting their potential for clinical application. Moreover, we identified organ-specific molecular bases and modifiable factors that could inspire innovative strategies for slowing aging.

Methods

Participants

The UK Biobank is one of the largest population-based biomedical cohorts that consists of more than 500,000 participants aged 40 to 96 across the UK[40,41]. All individuals undergoing retinal OCT at baseline or participating in the imaging visit for brain MRI, heart MRI, abdominal MRI, and whole-body dual-energy X-ray absorptiometry (DXA) scanning were initially included in the present study. In accordance with the Declaration of Helsinki, UKB received approval from the National Information Governance Board for Health and Social Care and the National Health Service North West Centre for Research Ethics Committee (Ref11:/NW/0382), and written informed consent was obtained from all participants. Clinical trial number is not applicable. Supplementary Information.

Multi-organ imaging phenotypes

The chronological age prediction for seven organs was constructed using 1777 IDPs of the corresponding organs, including the brain, heart, body composition, kidney, liver, pancreas, and eye. Brain gray matter and white matter were assessed separately. Only structural and functional IDPs of organs were selected and sourced from UKB (Supplementary Table 1).

Specifically, for the brain, the T1-weighted MRI was utilized to quantify 1010 IDPs related to regional grey matter volume, cortical mean thickness, and surface area. The diffusion-weighted MRI generated 443 measurements of white matter volume and microstructure of major white matter tracts. The microstructure measurements were characterized using diffusion tensor imaging (DTI) fitting and Neurite Orientation Dispersion and Density Imaging (NODDI) modelling[42], including fractional anisotropy (FA), mean diffusivity (MD), tensor mode (MO), L1, L2, L3, intra-cellular volume fraction (ICVF), isotropic or free water volume fraction (ISOVF) and orientation dispersion index (OD). For the heart, a set of cardiovascular MRI sequences was leveraged to assess 106 IDPs related to cardiac and aortic structure and function[43]. Besides, the abdominal MRI of multiple sequences was applied to generate volume, fat, and iron measurements in the liver, kidney, pancreas, and adipose tissue[44,45]. Meanwhile, 138 IDPs of body composition were measured from the DXA instrument. The measurements of bone area, bone mineral content, bone mineral density, lean mass, and fat mass were directly derived. Finally, 64 IDPs of the eye were derived from retinal OCT[46], which provides information about the thickness of retinal layers and subfields, along with the vertical cup-to-disc ratio and disc diameter.

For each organ, only participants with non-missing values for all IDPs required in the corresponding analyses were included. In other words, the participants with missing data for any organ-related IDPs were excluded, resulting in a slightly different number of healthy participants eligible for further age modelling (Supplementary Table 2).

Normative organ aging models

Least Absolute Shrinkage and Selection Operator regression (LASSO) models were trained in healthy participants to predict the chronological age of participants, with imaging-derived phenotypes of brain GM, brain WM, heart, body composition, kidney, liver, pancreas, and eye as potential predictors (Supplementary Table 1). The healthy status was defined as having no lifetime occurrence record in linked primary care, hospital inpatient, death register and self-reported medical condition sources (Category 1712). For each organ, the LASSO predictive model was constructed using a nested 10-fold cross-validation. The inner loop includes a cross-validation in selecting the best hyperparameter lambda, while the outer loop assessed the model's generalization performance by training the model on nine of the folds with the optimal lambda and tested on the one remaining fold. This cross-validation procedure resulted in a predicted age for each healthy individual. Following the suggestion, chronological age was also regressed from the predicted age in the training data, and the same regression model was applied to test data[47,48]. Model performance was evaluated by calculating Pearson's correlation coefficient (R) and mean absolute error (MAE) between predicted age and chronological age in the test sets.

Finally, eight optimal organ-specific biological age prediction models were created in healthy participants, and the models were applied to the remaining UKB participants to obtain the predicted age of each organ. The difference between the predicted age (i.e., biological age) of each organ and chronological age was regarded as the organ-specific age gap, informing whether the organ exhibited an accelerated or decelerated aging process compared to healthy peers. The bias-adjustment step substantially reduced the associations between chronological age and age gaps for brain GM (uncorrected slope: −0.34; corrected slope: −0.04), brain WM (uncorrected slope: −0.36; corrected slope: −0.04), heart (uncorrected slope: −0.45; corrected slope: −0.02), body composition (uncorrected slope: −0.46; corrected slope: −0.04), kidney (uncorrected slope: −0.89; corrected slope: −0.04), liver (uncorrected slope: −0.92; corrected slope: −0.06), pancreas (uncorrected slope: −0.91; corrected slope: −0.09) and eye (uncorrected slope: −0.92; corrected slope: −0.07). In sensitivity analysis, separate models were trained for healthy males and females to examine the potential sex difference in age prediction. Furthermore, to evaluate the generalizability of the model across different age bands and ancestries, we stratified healthy participants into two age groups (≤65 years and >65 years) and two ancestry groups (White and non-White). For each stratification, the model was trained in one subgroup and evaluated in the other subgroup.

Structural equation modeling

Structural equation modeling (SEM) was employed to assess the association between the age gap of one organ and that of another. Given that the eye was scanned at a different visit compared to other organs, the SEM was limited to six organs, except the eye. In determining the optimal model structure, the fast-greedy equivalence search (FGES) heuristic algorithm from Tetrad v7.6.5[49] was used to determine the causal Bayesian network with the highest score, which is useful in exploratory analyses to generate hypotheses about network structures of cross-sectional data. With the resulting network structure, pathway analysis was performed using lavaan v0.6.17 to estimate the strength and significance of the associations for edges in the final network. In sensitivity analysis, age at the imaging visit, sex, and the imaging site were further regressed from all organ-specific age gaps, and the search algorithm was performed on the resulting residuals. Due to the limited availability of repeated imaging visits, the SEM analyses were restricted to cross-sectional associations and do not permit inference about longitudinal effects or causal pathways.

The FGES–SEM analyses rely on several assumptions, including causal sufficiency (i.e., no unmeasured confounding), acyclic relationships without feedback loops, and the adequacy of a directed acyclic graph to represent conditional dependencies. In complex biological systems such as multi-organ aging, these assumptions are unlikely to be fully satisfied due to feedback mechanisms and latent factors. Therefore, the inferred network structures and path coefficients should be interpreted as statistical associations compatible with certain dependency structures, rather than evidence of causal effects, and are intended to be exploratory and hypothesis-generating.

Prediction of disease and mortality risk

A total of 13 categories of incident outcomes (Supplementary Table 6) were selected from UKB, including 12 broad categories of diseases (36 specific diseases) and all-cause mortality (four cause-specific mortality). The associations between the organ-specific age gaps and incident outcomes were tested with Cox proportional hazards models using R package survival v3.5.5. For all incident outcomes of 13 categories, the survival model included organ-specific age gap, chronological age, sex, years of education, body mass index (BMI), smoking, and drinking status as predictors. The significance of the effect of the age gaps was determined by FDR-corrected $P < 0.05$ across all pairs of organs and outcomes. The average age gap across organs was used to demonstrate the association between the overall age gap and the risk of incident outcomes. The Harrell's C-index was utilized to evaluate the model's ability to distinguish between patients who experience an event and those who do not, with higher values indicating better performance. We further calculated the change in Harrell's C-index (ΔC-index) when incorporating each organ age gap into the baseline model (which includes age, sex, and established conventional risk factors), with significance examined using 1000 bootstraps. A sensitivity analysis was conducted by regressing the effect of chronological age, sex, and scanning site prior to survival analysis. To enhance the reliability of the results, we also constructed the survival model by grouping organ-specific age gaps into quartiles from lowest to highest and assessed the ability of the age gaps for the risk stratification of diseases and mortality. To be rigorous, we further performed a sensitivity analysis that explicitly distinguishing confirmatory from exploratory results. Specifically, in confirmatory analysis, the associations between the seven organ-specific age gaps and the pre-specified organ-specific diseases underwent a strict Bonferroni-corrected $P < 0.05$. In exploratory analysis, we performed hierarchical FDR correction by accounting for inherent dependencies among tests and the false discovery rate was controlled within each organ. Specifically, for each of the eight organs, an omnibus p-value was computed using the Simes test based on the disease-specific p-values. The eight omnibus p-values were then FDR-corrected at 5%. Only organs with significant omnibus tests were considered further, and within each significant organ, associations were tested at FDR-corrected $P < 5\%$. Finally, we compared the strength of associations between high-accuracy and low-accuracy aging clocks. In particular, using a R threshold of 0.5, we categorized the organs into high-accuracy and low-accuracy groups. The HR estimates in survival analysis were compared between the two groups.

In further illustrating the clinical relevance of the organ-specific age gap, we developed the prediction model of diseases and mortality. For disease prediction analyses, incident cases were defined as participants who received a first diagnosis during follow-up after imaging. For each disease, controls were defined as participants who did not develop the disease during the follow-up period. Events occurring before imaging were excluded to ensure a clear temporal separation between predictors and outcomes. This design ensured that all prediction models were trained and evaluated using baseline imaging-derived measures to predict future disease risk. Specifically, the outcomes were defined as the lifelong incidents of diseases and mortality in UKB. For each organ, the top 50% IDPs contributing to the biological age model were selected as predictors, and the LightGBM predictive model was constructed using a 10-fold cross-validation framework to avoid potential overfitting. To mitigate the potential for highly correlated or redundant features, the LASSO model was leveraged to perform feature selection prior to disease prediction. Moreover, for overall prediction incorporating all organs, we further addressed potential collinearity using the *usdm* package, and only features with a variance inflation factor less than 10 were maintained. The resulting features were then used to construct the disease prediction model. Overall model performance was evaluated by averaging AUC across 10 folds. Using the same framework, an overall

prediction model including the selected predictors of all organs was also conducted. By comparing the performance of the established models to the baseline model that included only chronological age and sex, we evaluate whether the models that incorporated information about organ-specific biological age could more accurately predict further risk of diseases and mortality than traditional chronological age. To further evaluate the model robustness, we conducted a sensitivity analysis that split 70% of the data as training data and the resting 30% data as hold-out test set. Similar feature selection to that of 10-fold cross-validation was applied.

Association with proteins and blood biomarkers

The baseline plasma samples were processed using a NovaSeq 6000 Sequencing Systems, and the Olink Explore 3072 was utilized to quantify the concentration of 2923 unique proteins[50,51]. Three proteins (GLIPR1, NPM1, and PCOLCE) with a 25% or higher missing rate were discarded. The plasma samples were also prepared and processed to quantify blood biochemistry, blood count, and metabolic biomarkers[52]. Finally, for different organs, 530 to 5525 participants with all 2920 proteins (Supplementary Table 18) and 2569 to 25,241 participants with all 310 blood biomarkers available were included (Supplementary Table 14 and Supplementary Table 15). For both proteome and metabolites, the concentration of biomarkers was inverse-rank normalized, and the effects of chronological age and sex were removed.

For each organ, a generalized linear model was employed to examine the association between plasma protein and organ-specific age gaps, with the chronological age at imaging, sex, years of education, Townsend index, smoking status at imaging, drinking status at imaging, ethnicity, and the interval between baseline and imaging included as covariates. The significance was determined by FDR-corrected $P < 0.05$ across all 2920×7 protein-organ pairs. For each organ, GO biological processes enrichment was performed with an over-representation analysis from ToppGene. Tissue enrichment analysis was conducted with a hypergeometric test from FUMA v1.5.2, using gene expression from GTEx v8. A sensitivity analysis that constructed linear models with scanning site as an additional covariate was performed. Similar generalized linear models were performed for blood biochemistry, blood count, and metabolic biomarkers. The significance was determined by FDR-corrected $P < 0.05$ across all 310×7 blood biomarker-organ pairs. Similar to above, the beta estimates in association with biomarkers were compared between high-accuracy and low-accuracy aging clocks.

Phenome-wise association analysis

Taking similar UKB fields of modifiable factors as previous research[53], after excluding multinomial phenotypes, 143 common factors were obtained for organs except the eye, and 139 common factors were obtained for all organs.

PheWAS associations were examined with the PHESANT package in R[54]. In this study, the association between organ-specific age gap and factors was examined for each organ, with age and sex as covariates. The significance was determined by FDR-corrected $P < 0.05$ across 143×7 factor-organ pairs. In sensitivity analysis, we performed PheWAS with the 139 modifiable factors available for all eight organs, with significance determined by FDR-corrected $P < 0.05$ across 139×8 factor-organ pairs.

Genetic associations and drug target identification

To examine whether our findings could inform potential drug target for organ aging, we employed a two-sample *cis*-MR analysis for the causal associations between proteins and imaging-based organ-specific aging using TwoSampleMR R package, with statistical significance determined at a threshold of FDR-corrected $P < 0.05$. The GWAS analysis of organ-specific aging was performed by PLINK2 after excluding those subjects with proteomic data in UKB. The plasma and cerebrospinal fluid protein quantitative trait loci relationships were obtained from the UK Biobank Pharma Proteomics Project (http://ukb-ppp.gwas.eu)[51] and Cruchaga et al.[55], respectively. We selected cis-SNPs (located within 1 Mb of the transcription start site of the protein-encoding gene) that were significantly associated with plasma protein levels at a threshold of $P < 5 \times 10^{-8}$. Four MR methods were applied: inverse variance weighted (IVW), MR-Egger, weighted median, and weighted mode, with IVW as the primary method for reporting results. The Wald ratio was applied when only a single IV was available. Reverse MR analysis was conducted to confirm the causal effect of the protein on organ aging. To address potential pleiotropy, we employed sensitivity analyses using MR-PRESSO for detecting horizontal pleiotropy and MR-Egger analysis for directional pleiotropy. To further explore the therapeutic potential of our findings, we utilized the Genome for REPositioning drugs (GREP) software and Drug–Gene Interaction Database (https://dgidb.org/) to analyze the enrichment of MR-identified protein-encoding genes within the target genes of approved drugs.

Data availability

The plasma proteomic, metabolic, imaging, health outcomes, and phenotype data are publicly available at the official website of UK Biobank (http://www.ukbiobank.ac.uk/) and were used following the application no. 19542 and 202239.

Code availability

All software and methods used in our study are publicly available and described in the Methods. The code for the main analysis of this study is publicly available at https://github.com/hitrp/MultiOrganImagingAging/.

Received: 14 October 2025; Accepted: 14 February 2026;
Published online: 25 February 2026

References

1. Elliott, M. L. et al. Disparities in the pace of biological aging among midlife adults of the same chronological age have implications for future frailty risk and policy. *Nat. Aging* **1**, 295–308 (2021).
2. Rutledge, J., Oh, H. & Wyss-Coray, T. J. N. R. G. Measuring biological age using omics data. *Nat. Rev. Genet.* **23**, 715–727 (2022).
3. Liu, W. S. et al. Association of biological age with health outcomes and its modifiable factors. *Aging cell* **22**, e13995 (2023).
4. Tian, Y. E. et al. Heterogeneous aging across multiple organ systems and prediction of chronic disease and mortality. *Nat. Med.* **29**, 1221–1231 (2023).
5. Oh, H. S.-H. et al. Organ aging signatures in the plasma proteome track health and disease. *Nature* **624**, 164–172 (2023).
6. Goeminne, L. J. E. et al. Plasma protein-based organ-specific aging and mortality models unveil diseases as accelerated aging of organismal systems. *Cell Metab.* **37**(1), 205–222.e206 (2025).
7. Peng, H., Gong, W., Beckmann, C. F., Vedaldi, A. & Smith, S. M. Accurate brain age prediction with lightweight deep neural networks. *Med. Image Anal.* **68**, 101871 (2021).
8. Moguilner, S. et al. Brain clocks capture diversity and disparities in aging and dementia across geographically diverse populations. *Nat. Med.* **30**, 3646–3657 (2024).
9. More, S. et al. Brain-age prediction: a systematic comparison of machine learning workflows. *Neuroimage* **270**, 119947 (2023).
10. Gaser, C., Kalc, P. & Cole, J. H. A perspective on brain-age estimation and its clinical promise. *Nat. Comput. Sci.* **4**, 744–751 (2024).
11. Nanda, S. S., An, S. S. & Yi, D. K. Measurement of creatinine in human plasma using a functional porous polymer structure sensing motif. *Int. J. Nanomed.* **10**, 93–99 (2015).
12. West, M. et al. Circulating cystatin C is an independent risk marker for cardiovascular outcomes, development of renal impairment, and long-term mortality in patients with stable coronary heart disease: the LIPID study. *J. Am. Heart Assoc.* **11**, e020745 (2022).
13. Miller, M. et al. Triglycerides and cardiovascular disease: a scientific statement from the American Heart Association. *Circulation* **123**, 2292–2333 (2011).
14. Laufs, U., Parhofer, K. G., Ginsberg, H. N. & Hegele, R. A. Clinical review on triglycerides. *Eur. heart J.* **41**, 99–109c (2020).

15. Bryant, A. G. et al. Cerebrovascular senescence is associated with tau pathology in Alzheimer's disease. *Front. Neurol.* **11**, 575953 (2020).
16. Monstein, H. J., Grahn, N., Truedsson, M. & Ohlsson, B. Progastrin-releasing peptide and gastrin-releasing peptide receptor mRNA expression in non-tumor tissues of the human gastrointestinal tract. *World J. Gastroenterol.* **12**, 2574–2578 (2006).
17. Pendharkar, S. A., Drury, M., Walia, M., Korc, M. & Petrov, M. S. Gastrin-releasing peptide and glucose metabolism following pancreatitis. *Gastroenterol. Res.* **10**, 224–234 (2017).
18. Mazzoni, F., Dun, Y., Vargas, J. A., Nandrot, E. F. & Finnemann, S. C. Lack of the antioxidant enzyme methionine sulfoxide reductase A in mice impairs RPE phagocytosis and causes photoreceptor cone dysfunction. *Redox Biol.* **42**, 101918 (2021).
19. Olinger, E. et al. An intermediate-effect size variant in UMOD confers risk for chronic kidney disease. *Proc. Natl. Acad. Sci. USA* **119**, e2114734119 (2022).
20. Trudu, M. et al. Common noncoding UMOD gene variants induce salt-sensitive hypertension and kidney damage by increasing uromodulin expression. *Nat. Med.* **19**, 1655–1660 (2013).
21. Randles, M. J. et al. Identification of an altered matrix signature in kidney aging and disease. *J. Am. Soc. Nephrol.* **32**, 1713–1732 (2021).
22. Argentieri, M. A. et al. Proteomic aging clock predicts mortality and risk of common age-related diseases in diverse populations. *Nat. Med.* **30**, 2450–2460 (2024).
23. Zhang, S. et al. A metabolomic profile of biological aging in 250,341 individuals from the UK Biobank. *Nat. Commun.* **15**, 8081 (2024).
24. Duan, R., Fu, Q., Sun, Y. & Li, Q. Epigenetic clock: a promising biomarker and practical tool in aging. *Ageing Res. Rev.* **81**, 101743 (2022).
25. Yu, Z. et al. Thermal facial image analyses reveal quantitative hallmarks of aging and metabolic diseases. *Cell Metab.* **36**, 1482–1493.e1487 (2024).
26. Buckley, M. T. et al. Cell-type-specific aging clocks to quantify aging and rejuvenation in neurogenic regions of the brain. *Nat. Aging* **3**, 121–137 (2023).
27. Silvani, A., Calandra-Buonaura, G., Dampney, R. A. L. & Cortelli, P. Brain–heart interactions: physiology and clinical implications. *Philos. Trans. A Math. Phys. Eng. Sci.* **374**, 20150181 (2016).
28. Levine, G. N. et al. Psychological Health, Well-Being, and the Mind-Heart-Body Connection: a scientific statement From the American Heart Association. *Circulation* **143**, e763–e783 (2021).
29. Kivipelto, M. et al. Risk score for the prediction of dementia risk in 20 years among middle aged people: a longitudinal, population-based study. *Lancet Neurol.* **5**, 735–741 (2006).
30. Walters, K. et al. Predicting dementia risk in primary care: development and validation of the Dementia Risk Score using routinely collected data. *BMC Med.* **14**, 6 (2016).
31. Anstey, K. J., Cherbuin, N. & Herath, P. M. Development of a new method for assessing global risk of Alzheimer's disease for use in population health approaches to prevention. *Prev. Sci.* **14**, 411–421 (2013).
32. Tilg, H., Adolph, T. E., Dudek, M. & Knolle, P. Non-alcoholic fatty liver disease: the interplay between metabolism, microbes and immunity. *Nat. Metab.* **3**, 1596–1607 (2021).
33. Balzer, M. S., Rohacs, T. & Susztak, K. How many cell types are in the kidney and what do they do. *Annu. Rev. Physiol.* **84**, 507–531 (2022).
34. Atkinson, M. A., Campbell-Thompson, M., Kusmartseva, I. & Kaestner, K. H. Organisation of the human pancreas in health and in diabetes. *Diabetologia* **63**, 1966–1973 (2020).
35. Wang, D. et al. GDF15: emerging biology and therapeutic applications for obesity and cardiometabolic disease. *Nat. Rev. Endocrinol.* **17**, 592–607 (2021).
36. Guo, Y. et al. Plasma proteomic profiles predict future dementia in healthy adults. *Nat. Aging* **4**, 247–260 (2024).
37. Kashani, K., Rosner, M. H. & Ostermann, M. Creatinine: from physiology to clinical application. *Eur. J. Intern. Med.* **72**, 9–14 (2020).
38. Li, X. et al. Inflammation and aging: signaling pathways and intervention therapies. *Signal Transduct. Target. Ther.* **8**, 239 (2023).
39. Baechle, J. J. et al. Chronic inflammation and the hallmarks of aging. *Mol. Metab.* **74**, 101755 (2023).
40. Sudlow, C. et al. UK biobank: an open access resource for identifying the causes of a wide range of complex diseases of middle and old age. *PLoS Med.* **12**, e1001779 (2015).
41. Bycroft, C. et al. The UK Biobank resource with deep phenotyping and genomic data. *Nature* **562**, 203–209 (2018).
42. Lucignani, M. et al. Reliability on multiband diffusion NODDI models: a test retest study on children and adults. *Neuroimage* **238**, 118234 (2021).
43. Raisi-Estabragh, Z., Harvey, N. C., Neubauer, S. & Petersen, S. E. Cardiovascular magnetic resonance imaging in the UK Biobank: a major international health research resource. *Eur. Heart J. Cardiovasc. Imaging* **22**, 251–258 (2021).
44. Nauffal, V. et al. Noninvasive assessment of organ-specific and shared pathways in multi-organ fibrosis using T1 mapping. *Nat. Med.* **30**, 1749–1760 (2024).
45. Langner, T., Martínez Mora, A., Strand, R., Ahlström, H. & Kullberg, J. MIMIR: deep regression for automated analysis of UK biobank MRI scans. *Radiol. Artif. Intell.* **4**, e210178 (2022).
46. Warwick, A. N. et al. UK Biobank retinal imaging grading: methodology, baseline characteristics and findings for common ocular diseases. *Eye* **37**, 2109–2116 (2023).
47. Smith, S. M., Vidaurre, D., Alfaro-Almagro, F., Nichols, T. E. & Miller, K. L. Estimation of brain age delta from brain imaging. *Neuroimage* **200**, 528–539 (2019).
48. Le, T. T. et al. A nonlinear simulation framework supports adjusting for age when analyzing BrainAGE. *Front. Aging Neurosci.* **10**, 317 (2018).
49. Ramsey, J. D. & Andrews, B. Py-Tetrad and RPy-Tetrad: a new python interface with R support for tetrad causal search. *Proc. Mach. Learn. Res.* **223**, 40–51 (2023).
50. Dhindsa, R. S. et al. Rare variant associations with plasma protein levels in the UK Biobank. *Nature* **622**, 339–347 (2023).
51. Sun, B. B. et al. Plasma proteomic associations with genetics and health in the UK Biobank. *Nature* **622**, 329–338 (2023).
52. Julkunen, H. et al. Atlas of plasma NMR biomarkers for health and disease in 118,461 individuals from the UK Biobank. *Nat. Commun.* **14**, 604 (2023).
53. Zhang, B. et al. Identifying behaviour-related and physiological risk factors for suicide attempts in the UK Biobank. *Nat. Hum. Behav.* **8**, 1784–1797 (2024).
54. Millard, L. A. C., Davies, N. M., Gaunt, T. R., Davey Smith, G. & Tilling, K. Software application profile: PHESANT: a tool for performing automated phenome scans in UK Biobank. *Int. J. Epidemiol.* **47**, 29–35 (2018).
55. Western, D. et al. Proteogenomic analysis of human cerebrospinal fluid identifies neurologically relevant regulation and implicates causal proteins for Alzheimer's disease. *Nat. Genet.* **56**, 2672–2684 (2024).

Acknowledgements

H.W. was supported by grants from the National Natural Science Foundation of China (No. 62331021). W.C. was supported by grants from the Noncommunicable Chronic Diseases-National Science and Technology Major Project (2025ZD0546300), the National Key R&D Program of China (No. 2023YFC3605400), the National Natural Science Foundation of China (No. 82472055, No. 62433008), the Shanghai Pilot Program for Basic Research—Fudan University 21TQ1400100 (25TQ010), and Shanghai Science and Technology Commission Program (23JS1410100). J.-T.Y. was supported by grants from the Science and Technology Innovation 2030 Major Projects (no. 2022ZD0211600), the National Natural Science Foundation of China (nos 82071201, 81971032 and 92249305), the Shanghai Municipal Science and Technology Major Project (no. 2018SHZDZX01), the Research Start-Up Fund of Huashan Hospital (no. 2022QD002), the Excellence 2025 Talent Cultivation Program at Fudan University (no.

3030277001), Shanghai Talent Development Funding for the Project (no. 2019074), and the Zhangjiang Lab, Tianqiao and Chrissy Chen Institute, and the State Key Laboratory of Neurobiology and Frontiers Center for Brain Science of Ministry of Education, Fudan University. J.-F.F. was supported by the National Key R&D Program of China (nos 2018YFC1312904 and 2019YFA0709502), the Shanghai Municipal Science and Technology Major Project (no. 2018SHZDZX01), the 111 Project (no. B18015), the Shanghai Center for Brain Science and Brain-Inspired Technology and the Zhangjiang Lab. P.R. was funded by China Postdoctoral Science Foundation (2025M772197 and GZC20230530). We thank all participants and team members of the UK Biobank. All icons were created with BioRender.com. The funders had no role in study design, data collection and analysis or preparation of the manuscript.

Author contributions

W.C., J.Y., and H.W.: Conceptualization, supervision, project administration, writing—reviewing and editing, and funding acquisition. P.R.: Software, formal analysis, hardware, validation, data analysis, and writing—original draft preparation, reviewing and editing. W.S.: Formal analysis and visualization. J.Y. and Y.L.: Methodology, formal analysis, and writing—reviewing and editing. W.G., W.Z., Z.Z., X.H., W.L., and J.F.: Methodology and writing—reviewing and editing. F.D.: Hardware and technique support. All authors have read and approved the manuscript.

Competing interests

The authors declare no competing interests.

Additional information

Supplementary information The online version contains supplementary material available at https://doi.org/10.1038/s41746-026-02488-7.

Correspondence and requests for materials should be addressed to He Wang, Jin-Tai Yu or Wei Cheng.